

Path-lifting Mechanism for MRP and Equivalence of Stability between results in $\bar{\mathbb{R}}^3$ and $\text{SO}(3)$

Luís Martins, Carlos Cardeira, and Paulo Oliveira

February 7, 2023

Abstract

The modified Rodrigues parameters (MRP) are a less explored attitude representation characterized by two numerically different triplets that are infinite for different principal rotations. By judiciously switching between these triplets, the MRP yield a minimal non-singular attitude description with advantageous inherent properties that an increasing number of control-related applications explore. The space of MRP results from the Alexandroff compactification of \mathbb{R}^3 , $\bar{\mathbb{R}}^3$, which, similar to the space of unit quaternions, is a double cover of the rotation group $\text{SO}(3)$. In this direction, this technical report highlights some instrumental properties of the corresponding covering map and proposes a hybrid dynamic path-lifting algorithm to uniquely and consistently extract the MRP vector from a given rotation matrix. The resulting output evolves inside a three-dimensional unit sphere enclosed by a hysteresis region. With this hybrid algorithm in place, a theoretical basis for equivalence of stability between results in the base space $\text{SO}(3)$ and the covering space $\bar{\mathbb{R}}^3$ is developed. To this end, two closed-loop hybrid systems are formulated: one encompassing the lifted attitude dynamics and the other encapsulating the attitude dynamics described in the base space and the hybrid path-lifting algorithm. As the main contribution, this report demonstrates that an asymptotic stability result obtained with a feedback controller designed in the covering space for the former system translates into an equivalent asymptotic stability result in the base space when the same feedback controller is applied to the latter hybrid system.

Notation and Preliminaries

\mathbb{R}^n represents the n -dimensional Euclidean space; $\mathbb{R}_{\geq 0}$ expresses the set of non-negative real numbers; $\mathbb{R}^{n \times m}$ denotes the set of $n \times m$ matrices; $\mathbb{S}^n = \{\mathbf{x} \in \mathbb{R}^{n+1} : \mathbf{x}^\top \mathbf{x} = 1\}$ symbolizes the n -dimensional unit sphere; $\mathbf{I}_n \in \mathbb{R}^{n \times n}$ represents the n -dimensional identity matrix; $K\mathbb{B}^n$ denotes the closed ball of radius K centered at the origin of \mathbb{R}^n . The set $\bar{\mathbb{R}}^n := \mathbb{R}^n \cup \{\infty\}$ results from

the inclusion map $\mathbf{c} : \mathbb{R}^n \mapsto \bar{\mathbb{R}}^n$ and is often referred to as the one-point compactification or Alexandroff compactification of \mathbb{R}^n . Given two functions $\mathbf{f} : \mathcal{X} \mapsto \mathcal{Y}$ and $\mathbf{g} : \mathcal{Y} \mapsto \mathcal{Z}$, $\mathbf{g} \circ \mathbf{f} = \mathbf{g}(\mathbf{f}) : \mathcal{X} \mapsto \mathcal{Z}$ denotes the composite function \mathbf{g} of \mathbf{f} ; $\mathbf{e}_i \in \mathbb{R}^3$ denotes a vector of zeros except for the i^{th} entry which is 1; $[\boldsymbol{\omega}]_{\times}$ is such that $[\boldsymbol{\omega}]_{\times} \mathbf{s} = \boldsymbol{\omega} \times \mathbf{s}$ for each $\mathbf{s}, \boldsymbol{\omega} \in \mathbb{R}^3$, where \times denotes the cross product. Given a vector $\mathbf{s} \in \mathbb{R}^n$ and a closed set $\mathcal{A} \subset \mathbb{R}^n$, $\|\mathbf{s}\|_{\mathcal{A}}$ denotes the distance of \mathbf{s} to \mathcal{A} and is given by $\|\mathbf{s}\|_{\mathcal{A}} := \inf_{\mathbf{x} \in \mathcal{A}} \|\mathbf{s} - \mathbf{x}\|$.

Concerning rigid-body attitude description, \mathbf{R} represents an element of the three-dimensional special orthogonal group $\text{SO}(3)$ and corresponds to the rotation matrix from the body-fixed frame to the inertial frame. The underlying kinematic and dynamic equations for the rotation of a rigid body are, respectively,

$$\dot{\mathbf{R}} = \mathbf{R} [\boldsymbol{\omega}]_{\times} \quad (1a)$$

$$\mathbf{J} \dot{\boldsymbol{\omega}} = [\mathbf{J} \boldsymbol{\omega}]_{\times} \boldsymbol{\omega} + \boldsymbol{\tau} \quad (1b)$$

where $\boldsymbol{\omega} \in \mathbb{R}^3$ symbolizes the angular velocity expressed in the body-fixed frame, $\boldsymbol{\tau} \in \mathbb{R}^3$ denotes the torque input, $\mathbf{J} \in \mathbb{R}^{3 \times 3}$ models the symmetric tensor of inertia of the rigid body.

The vector $\mathbf{q} \in \mathbb{S}^3$ denotes the unit quaternion and is defined by the pair (q_0, \mathbf{q}_1) , where $q_0 \in \mathbb{R}$ and $\mathbf{q}_1 \in \mathbb{R}^3$ correspond, respectively, to the scalar and vector components. The map $\mathcal{R} : \mathbb{S}^3 \mapsto \text{SO}(3)$ is defined as

$$\mathcal{R}(\mathbf{q}) = \mathbf{I}_3 + 2q_0 [\mathbf{q}_1]_{\times} + 2[\mathbf{q}_1]_{\times}^2 \quad (2)$$

which satisfies $\mathcal{R}(\mathbf{q}) = \mathcal{R}(-\mathbf{q})$. The double-valued inverse map $\mathcal{Q} : \text{SO}(3) \rightrightarrows \mathbb{S}^3$ is characterized as

$$\mathcal{Q}(\mathbf{R}) = \{\mathbf{q} \in \mathbb{S}^3 : \mathcal{R}(\mathbf{q}) = \mathbf{R}\} \quad (3)$$

In addition to the previous representations, the MRP vector, $\boldsymbol{\vartheta} \in \bar{\mathbb{R}}^3$, can also be used to parameterize the attitude. Each $\boldsymbol{\vartheta}$ has a shadow MRP associated, $\boldsymbol{\vartheta}^s \in \bar{\mathbb{R}}^3$. Both $\boldsymbol{\vartheta}$ and $\boldsymbol{\vartheta}^s$ are related to a given unit quaternion through

$$\boldsymbol{\vartheta} = \begin{cases} \frac{\mathbf{q}_1}{1+q_0} & , \text{ for } \mathbf{q} \in \mathbb{S}^3 \setminus \{\mathbf{s}\} \\ \infty & , \text{ for } \mathbf{q} \in \{\mathbf{s}\} \end{cases} \quad (4a)$$

$$\boldsymbol{\vartheta}^s = \begin{cases} \frac{-\mathbf{q}_1}{1-q_0} & , \text{ for } \mathbf{q} \in \mathbb{S}^3 \setminus \{\mathbf{n}\} \\ \infty & , \text{ for } \mathbf{q} \in \{\mathbf{n}\} \end{cases} \quad (4b)$$

where $\mathbf{s} = (-1, 0, 0, 0)$ and $\mathbf{n} = (1, 0, 0, 0)$ are, respectively, the south and north poles of the three-dimensional sphere. In virtue of the original and shadow sets being singular for different rotations, judiciously switching between the original and shadow sets yields a minimal non-singular attitude representation [Junkins and Schaub \(2009\)](#). The shadow set can be obtained from the original set by resorting to the map $\Upsilon : \bar{\mathbb{R}}^3 \mapsto \bar{\mathbb{R}}^3$:

$$\boldsymbol{\vartheta}^s = \Upsilon(\boldsymbol{\vartheta}) = \begin{cases} -\frac{\boldsymbol{\vartheta}}{\|\boldsymbol{\vartheta}\|^2} & , \text{ for } \boldsymbol{\vartheta} \in \bar{\mathbb{R}}^3 \setminus \{\mathbf{0}\} \\ \infty & , \text{ for } \boldsymbol{\vartheta} \in \{\mathbf{0}\} \\ \mathbf{0} & , \text{ for } \boldsymbol{\vartheta} \in \{\infty\} \end{cases} \quad (5)$$

Both the original and the shadow MRP respect the following kinematic equation [Junkins and Schaub \(2009\)](#)

$$\dot{\boldsymbol{\vartheta}} = \mathbf{T}(\boldsymbol{\vartheta})\boldsymbol{\omega} = \begin{cases} \frac{(1-\|\boldsymbol{\vartheta}\|^2)\mathbf{I}_3+2[\boldsymbol{\vartheta}]_{\times}+2\boldsymbol{\vartheta}\boldsymbol{\vartheta}^{\top}}{4} \boldsymbol{\omega} & , \text{ for } \boldsymbol{\vartheta} \in \mathbb{R}^3 \\ \infty & , \text{ for } \boldsymbol{\vartheta} \in \{\infty\} \end{cases} \quad (6)$$

The mapping $\mathcal{R}_{\boldsymbol{\vartheta}}(\boldsymbol{\vartheta}) : \bar{\mathbb{R}}^3 \mapsto \text{SO}(3)$

$$\mathcal{R}_{\boldsymbol{\vartheta}}(\boldsymbol{\vartheta}) := \begin{cases} \mathbf{I}_3 + \frac{8[\boldsymbol{\vartheta}]_{\times}^2+4(1-\|\boldsymbol{\vartheta}\|^2)[\boldsymbol{\vartheta}]_{\times}}{(1+\|\boldsymbol{\vartheta}\|^2)^2} & , \text{ for } \boldsymbol{\vartheta} \in \mathbb{R}^3 \\ \mathbf{I}_3 & , \text{ for } \boldsymbol{\vartheta} \in \{\infty\} \end{cases} \quad (7)$$

maps a given $\boldsymbol{\vartheta}$ to the corresponding rotation matrix. This map has the property $\mathcal{R}_{\boldsymbol{\vartheta}}(\boldsymbol{\vartheta}) = \mathcal{R}_{\boldsymbol{\vartheta}}(\boldsymbol{\vartheta}^s)$. For further details, the reader is referred to [Junkins and Schaub \(2009\)](#).

A hybrid system \mathcal{H} is characterized by the data $(\mathbf{C}, \mathbf{F}, \mathbf{D}, \mathbf{G})$ and its model can be represented by

$$\mathcal{H} \begin{cases} \dot{\mathbf{x}} \in \mathbf{F}(\mathbf{x}) & , \quad \mathbf{x} \in \mathbf{C} \\ \mathbf{x}^+ \in \mathbf{G}(\mathbf{x}) & , \quad \mathbf{x}^+ \in \mathbf{D} \end{cases} \quad (8)$$

The hybrid system evolves according to the set-valued map $\mathbf{F} : \mathbb{R}^n \rightrightarrows \mathbb{R}^n$ while in the flow set $\mathbf{C} \subset \mathbb{R}^n$ and instantaneously changes under the set-valued map $\mathbf{G} : \mathbb{R}^n \rightrightarrows \mathbb{R}^n$ while in the jump set $\mathbf{D} \subset \mathbb{R}^n$. A solution $\mathbf{x}(t, j)$ to \mathcal{H} , with t and j denoting, respectively, ordinary time and jump time, is a function $\mathbf{x} : \text{dom } \mathbf{x} \mapsto \mathbb{R}^n$, where $\text{dom } \mathbf{x} \subset \mathbb{R}_{\geq 0} \times \mathbb{N}$ is a hybrid time domain. For each fixed $j \in \mathbb{N}$ the function $t \mapsto \mathbf{x}(t, j)$ is locally absolutely continuous on the interval $\mathcal{T}_j := \{t : (t, j) \in \text{dom } \mathbf{x}\}$. For a given hybrid time domain, $\bar{T}(\mathbf{x}) = \sup \{t \in \mathbb{R}_{\geq 0} : \exists j \in \mathbb{N} \text{ such that } (t, j) \in \text{dom } \mathbf{x}\}$. The function $\mathbf{x}_{\downarrow t} : [0, \bar{T}(\mathbf{x})) \mapsto \mathbb{R}^n$ symbolizes the time projection of $\mathbf{x}(t, j)$ given by $\mathbf{x}_{\downarrow t} = \mathbf{x}(t, J(t))$, with $J(t) = \max \{j \in \mathbb{N} : (t, j) \in \text{dom } \mathbf{x}\}$. For further details, see [Goebel et al. \(2012\)](#).

1 Properties of the map $\mathcal{R}_\vartheta : \bar{\mathbb{R}}^3 \mapsto \text{SO}(3)$

To devise a hybrid methodology for dynamic path-lifting from $\text{SO}(3)$ to $\bar{\mathbb{R}}^3$ and establishing parallelisms in terms of stability results in these spaces, one has to ascertain whether the map $\mathcal{R}_\vartheta : \bar{\mathbb{R}}^3 \mapsto \text{SO}(3)$ possesses the necessary characteristics for those effects. Bearing in mind that \mathcal{R}_ϑ consists of the composition of \mathcal{R} and the inverse of the stereographic projections described in (4) and that the properties of \mathcal{R} are well-known from the literature, firstly, the focus is on showing that the stereographic projection from \mathbb{S}^3 to $\bar{\mathbb{R}}^3$ is a diffeomorphism. Afterwards, on the basis of this diffeomorphic relation, we apply known arguments from the literature for composite maps to draw conclusions regarding the required characteristics of \mathcal{R}_ϑ .

Let the manifold \mathbb{S}^3 be described by the atlas $\mathcal{A}_1 = \{(\mathbf{U}_n, \varphi_n), (\mathbf{U}_s, \varphi_s)\}$ where

$$\begin{aligned} \mathbf{U}_n &:= \mathbb{S}^3 \setminus \{\mathbf{n}\}, & \varphi_n &: \mathbf{U}_n \mapsto \mathbb{R}^3, & \varphi_n(\mathbf{q}) &:= \frac{-\mathbf{q}_1}{1 - q_0} \\ \mathbf{U}_s &:= \mathbb{S}^3 \setminus \{\mathbf{s}\}, & \varphi_s &: \mathbf{U}_s \mapsto \mathbb{R}^3, & \varphi_s(\mathbf{q}) &:= \frac{\mathbf{q}_1}{1 + q_0} \end{aligned}$$

The functions $\varphi_n(\mathbf{q})$ and $\varphi_s(\mathbf{q})$ correspond, respectively, to the stereographic projection of \mathbf{q} from the north pole of the sphere multiplied by -1 and the stereographic projection from the south pole. The referred functions verify the equality $\varphi_n(\mathbf{q}) = \varphi_s(-\mathbf{q})$. The inverse functions $\varphi_n^{-1} : \mathbb{R}^3 \mapsto \mathbf{U}_n$ and $\varphi_s^{-1} : \mathbb{R}^3 \mapsto \mathbf{U}_s$ are given by

$$\begin{aligned} \varphi_n^{-1}(\vartheta) &= \left(\frac{\|\vartheta\|^2 - 1}{1 + \|\vartheta\|^2}, \frac{-2\vartheta}{1 + \|\vartheta\|^2} \right) \\ \varphi_s^{-1}(\vartheta) &= \left(\frac{1 - \|\vartheta\|^2}{1 + \|\vartheta\|^2}, \frac{2\vartheta}{1 + \|\vartheta\|^2} \right) \end{aligned}$$

Further, φ_n and φ_s are continuous bijective maps with continuous inverse functions, being, thereby, homeomorphisms. Furthermore, since φ_n and φ_s map from one-punctured spheres to \mathbb{R}^3 , it follows that the pairs $(\mathbf{U}_n, \varphi_n)$ and $(\mathbf{U}_s, \varphi_s)$ are charts according to (Lee, 2013, p.4). Regarding the sets \mathbf{U}_n and \mathbf{U}_s , $\mathbf{U}_n \cap \mathbf{U}_s \neq \emptyset$ and $\mathbf{U}_n \cup \mathbf{U}_s$ covers \mathbb{S}^3 . Hence, the indexed family of charts $(\mathbf{U}_n, \varphi_n), (\mathbf{U}_s, \varphi_s)$ forms an atlas on \mathbb{S}^3 . The transition map $\Psi_1(\vartheta) : \mathbb{R}^3 \setminus \{\mathbf{0}\} \mapsto \mathbb{R}^3 \setminus \{\mathbf{0}\}$ yields

$$\Psi_1(\vartheta) = \varphi_s \circ \varphi_n^{-1}(\vartheta) = \frac{-\vartheta}{\|\vartheta\|^2},$$

which is identical to the mapping between the original and shadow sets, given in (5), for $\vartheta \in \mathbb{R}^3 \setminus \{\mathbf{0}\}$. Note that the transition map verifies $\Psi_1(\vartheta) = \Psi_1^{-1}(\vartheta)$. Thus, the transition map and its inverse are smooth and, consequently, the two charts are smoothly compatible and \mathcal{A}_1 is a smooth atlas for \mathbb{S}^3 (Lee, 2013, p.12).

Let the atlas $\mathcal{A}_2 = \{(\mathbf{U}_a, \varphi_a), (\mathbf{U}_b, \varphi_b)\}$ with

$$\mathbf{U}_a := \mathbb{R}^3, \quad \varphi_a : \mathbf{U}_a \mapsto \mathbb{R}^3, \quad \varphi_a(\vartheta) := \vartheta$$

$$\mathbf{U}_b := \bar{\mathbb{R}}^3 \setminus \{\mathbf{0}\}, \quad \varphi_b : \mathbf{U}_b \mapsto \mathbb{R}^3, \quad \varphi_b(\vartheta) := \Upsilon(\vartheta), \quad \text{for } \vartheta \in \mathbf{U}_b$$

describe the manifold $\bar{\mathbb{R}}^3$. To shed some light on the reasoning behind the choice of these functions, one might think of φ_a as the identity map for one of the MRP sets and φ_b as the map that enables computing the counterpart representation. The functions φ_a and φ_b are continuous bijective open mappings. The inverse of these functions, given by

$$\varphi_a^{-1} : \mathbb{R}^3 \mapsto \mathbf{U}_a, \quad \varphi_a^{-1}(\vartheta) = \vartheta$$

$$\varphi_b^{-1} : \mathbb{R}^3 \mapsto \mathbf{U}_b, \quad \varphi_b^{-1}(\vartheta) = \Upsilon(\vartheta), \quad \text{for } \vartheta \in \mathbb{R}^3$$

are continuous. Thus, φ_a and φ_b are homeomorphisms. The union $\mathbf{U}_a \cup \mathbf{U}_b$ covers $\bar{\mathbb{R}}^3$. Hence, in light of these properties, the charts $(\mathbf{U}_a, \varphi_a)$ and $(\mathbf{U}_b, \varphi_b)$ form an atlas on $\bar{\mathbb{R}}^3$. The transition map $\Psi_2(\vartheta) : \mathbb{R}^3 \setminus \{\mathbf{0}\} \mapsto \mathbb{R}^3 \setminus \{\mathbf{0}\}$ satisfies

$$\Psi_2(\vartheta) = \varphi_b \circ \varphi_a^{-1}(\vartheta) = \frac{-\vartheta}{\|\vartheta\|^2},$$

and

$$\Psi_2^{-1}(\vartheta) = \varphi_a \circ \varphi_b^{-1}(\vartheta) = \frac{-\vartheta}{\|\vartheta\|^2},$$

By virtue of Ψ_2 and Ψ_2^{-1} being smooth functions, the transition map is a diffeomorphism. Therefore, the two charts are smoothly compatible and \mathcal{A}_2 is a smooth atlas (Lee, 2013, p.12).

Consider the map $\varphi(\vartheta) : \bar{\mathbb{R}}^3 \mapsto \mathbb{S}^3$ defined as

$$\varphi(\vartheta) := \begin{cases} \varphi_s^{-1}(\vartheta) & , \quad \text{for } \vartheta \in \mathbb{R}^3 \\ \mathbf{s} & , \quad \text{for } \vartheta \in \{\infty\} \end{cases} \quad (11)$$

For the purpose of characterizing the smoothness of φ , the smooth atlas \mathcal{A}_1 and \mathcal{A}_2 are resorted to. In this direction, the following composite maps are constructed:

$$\Theta_1 : \varphi_b(\mathbf{U}_b \cap \varphi^{-1}(\mathbf{U}_n)) \mapsto \varphi_n(\mathbf{U}_n), \quad \Theta_1 := \varphi_n \circ \varphi_b^{-1}(\vartheta)$$

$$\Theta_2 : \varphi_a(\mathbf{U}_a \cap \varphi^{-1}(\mathbf{U}_s)) \mapsto \varphi_s(\mathbf{U}_s), \quad \Theta_2 := \varphi_s \circ \varphi \circ \varphi_a^{-1}(\vartheta)$$

which leads to $\Theta_1(\vartheta) = \vartheta$ and $\Theta_2(\vartheta) = \vartheta$. Hence, Θ_1 and Θ_s are smooth maps from \mathbb{R}^3 to \mathbb{R}^3 . It follows from (Lee, 2013, Proposition 2.5) that the map φ is smooth. Concerning the inverse function $\varphi^{-1} : \mathbb{S}^3 \mapsto \bar{\mathbb{R}}^3$, expressed as

$$\varphi^{-1}(\mathbf{q}) = \begin{cases} \varphi_s(\mathbf{q}) & , \quad \text{for } \mathbf{q} \in \mathbb{S}^3 \setminus \{\mathbf{0}\} \\ \infty & , \quad \text{for } \mathbf{q} \in \{\mathbf{s}\} \end{cases}, \quad (12)$$

in light of

$$\varphi_{\mathbf{b}} \circ \varphi^{-1} \circ \varphi_{\mathbf{n}}^{-1}(\vartheta) = (\varphi_{\mathbf{n}} \circ \varphi_{\mathbf{b}}^{-1})^{-1}(\vartheta) = \Phi_1^{-1}(\vartheta) = \vartheta$$

and

$$\varphi_{\mathbf{0}} \circ \varphi^{-1} \circ \varphi_{\mathbf{s}}^{-1}(\vartheta) = (\varphi_{\mathbf{s}} \circ \varphi \circ \varphi_{\mathbf{a}}^{-1})^{-1}(\vartheta) = \Phi_2^{-1}(\vartheta) = \vartheta,$$

the map φ^{-1} is also smooth (Lee, 2013, Proposition 2013). Therefore, one concludes that φ is a diffeomorphism from $\bar{\mathbb{R}}^3$ to \mathbb{S}^3 . As a result, the smooth manifolds $\bar{\mathbb{R}}^3$ and \mathbb{S}^3 are diffeomorphic.

The demonstrated equivalence relation between the smooth manifolds $\bar{\mathbb{R}}^3$ and \mathbb{S}^3 rooted in the diffeomorphism $\varphi(\vartheta) : \bar{\mathbb{R}}^3 \mapsto \mathbb{S}^3$ is instrumental to derive some crucial properties of the map $\mathcal{R}_{\vartheta} : \bar{\mathbb{R}}^3 \mapsto \text{SO}(3)$. In this direction, the derivation starts from a fairly known result: the manifold \mathbb{S}^3 is a covering space for $\text{SO}(3)$ with \mathcal{R} as covering map. In light of the map $\varphi(\vartheta) : \bar{\mathbb{R}}^3 \mapsto \mathbb{S}^3$ being a diffeomorphism, it follows from (Lee, 2013, Proposition 2.15) that this map is also a homeomorphism. Then, since any homeomorphism is trivially a covering map, the Alexandroff compactification $\bar{\mathbb{R}}^3$ is a covering space for \mathbb{S}^3 with $\varphi(\vartheta)$ as covering map. With these properties in mind, in conjunction with the notion that the map \mathcal{R}_{ϑ} results from the composition $\mathcal{R} \circ \varphi(\vartheta) : \bar{\mathbb{R}}^3 \mapsto \text{SO}(3)$ (Junkins and Schaub, 2009, p.120) and the fact that the inverse map of $\mathcal{R}(\mathbf{q})$, $\mathcal{Q} : \text{SO}(3) \rightrightarrows \mathbb{S}^3$, is finite for every $\mathbf{R} \in \text{SO}(3)$, it follows from (Munkres, 2000, p. 341) that $\mathcal{R}_{\vartheta} : \bar{\mathbb{R}}^3 \mapsto \text{SO}(3)$ is a covering map with $\bar{\mathbb{R}}^3$ and $\text{SO}(3)$ as covering and base spaces, respectively. Furthermore, according to (Lee, 2013, Proposition 4.6), the map $\varphi(\vartheta)$ is a local diffeomorphism and, by virtue of \mathcal{R} being also a local diffeomorphism, the composition map $\mathcal{R}_{\vartheta}(\vartheta)$ is itself a local diffeomorphism.

The proved properties of the map $\mathcal{R}_{\vartheta}(\vartheta)$, namely, being a covering map and a local diffeomorphism everywhere, are quite relevant: the former opens the door for the application of unique path-lifting methodologies (Munkres, 2000, Lemma 54.1.), whereas the latter allows preserving everywhere the local differentiable structure when mapping between $\bar{\mathbb{R}}^3$ and $\text{SO}(3)$. In Figure 1, the continuous mapping between the topological spaces $\bar{\mathbb{R}}^3$, \mathbb{S}^3 and $\text{SO}(3)$, as well as the corresponding elements describing the related attitude representation for a certain time instant, are schematically presented. Due to $\mathbf{R}(t)$ being a continuous mapping of $[0, 1]$ into $\text{SO}(3)$ and given that $\mathcal{R}_{\vartheta}(\vartheta)$ are $\mathcal{R}(\mathbf{q})$ are covering maps, $\vartheta(t)$ and $\mathbf{q}(t)$ are lifts of $\mathbf{R}(t)$. It is worth mentioning that the closed interval $[0, 1]$ was considered due to its extensive use in topology to represent a bounded time interval. Any other closed and bounded time interval could be considered for this purpose.

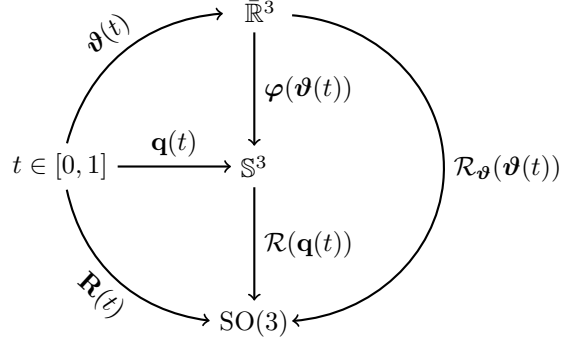


Figure 1: Scheme of the maps between the topological spaces $\bar{\mathbb{R}}^3$, \mathbb{S}^3 and $\text{SO}(3)$ and of the respective elements describing the associated attitude representation for a given time instant.

2 Hybrid Dynamic Path-lifting Algorithm for MRP extraction

For the purpose of extracting the MRP representation of the attitude, a hybrid algorithm is constructed to ensure the uniqueness and consistency of this operation. The algorithm extends the dynamic path-lifting solution proposed by [Mayhew et al. \(2013\)](#) with the inclusion of an additional state and application of stereographic projection to the smoothly lifted quaternion. Let the stereographic projection be defined by the smooth inverse function $\varphi^{-1}(\mathbf{q}) : \mathbb{S}^3 \mapsto \bar{\mathbb{R}}^3$ given in (4). Consider a discrete state $m \in \{-1, 1\}$ and a hysteretic parameter $\delta \in \mathbb{R}_{>0}$. Then, the following jump and map sets are defined

$$\mathbf{C}_m := \{(\hat{\mathbf{q}}, \mathbf{R}, m) \in \mathbb{S}^3 \times \text{SO}(3) \times \{-1, 1\} : \|\varphi^{-1}(m\Phi(\hat{\mathbf{q}}, \mathbf{R}))\| \leq 1 + \delta\} \quad (13)$$

$$\mathbf{D}_m := \{(\hat{\mathbf{q}}, \mathbf{R}, m) \in \mathbb{S}^3 \times \text{SO}(3) \times \{-1, 1\} : \|\varphi^{-1}(m\Phi(\hat{\mathbf{q}}, \mathbf{R}))\| \geq 1 + \delta\} \quad (14)$$

where, as proposed by [Mayhew et al. \(2013\)](#), $\Phi : \mathbb{S}^3 \times \text{SO}(3) \rightrightarrows \bar{\mathbb{R}}^3$ denotes the map

$$\Phi(\hat{\mathbf{q}}, \mathbf{R}) := \underset{\mathbf{p} \in \mathcal{Q}(\mathbf{R})}{\text{argmax}} \quad \hat{\mathbf{q}}^\top \mathbf{p} \quad , \quad (15)$$

and $\hat{\mathbf{q}} := (\hat{q}_0, \hat{\mathbf{q}}_1) \in \mathbb{S}^3$ symbolizes the memory state, which is updated in accordance with the following flow and jump maps

$$\mathbf{C}_1 := \{(\hat{\mathbf{q}}, \mathbf{R}, m) \in \mathbb{S}^3 \times \text{SO}(3) \times \{-1, 1\} : \text{dist}(\hat{\mathbf{q}}, \mathcal{Q}(\mathbf{R})) \leq \alpha\}, \quad (16)$$

and

$$\mathbf{D}_1 := \{(\hat{\mathbf{q}}, \mathbf{R}, m) \in \mathbb{S}^3 \times \text{SO}(3) \times \{-1, 1\} : \text{dist}(\hat{\mathbf{q}}, \mathcal{Q}(\mathbf{R})) \geq \alpha\}, \quad (17)$$

with $\alpha \in]0, 1[$ and $\text{dist}(\hat{\mathbf{q}}, \mathcal{Q}(\mathbf{R})) = \inf \{1 - \hat{\mathbf{q}}^\top \mathbf{p} : \mathbf{p} \in \mathcal{Q}(\mathbf{R})\}$, are also considered here. With these definitions in mind, the hybrid algorithm for the extraction of the MRP representation is described by the system \mathcal{H}_ϑ :

$$\mathcal{H}_\vartheta \left\{ \begin{array}{l} \dot{\hat{\mathbf{q}}} = 0, \quad \dot{m} = 0 \\ \hat{\mathbf{q}}^+ \in \Phi(\hat{\mathbf{q}}, \mathbf{R}), \quad m^+ = m \\ \hat{\mathbf{q}}^+ = \hat{\mathbf{q}}, \quad m^+ = -m \end{array} \right. , \quad \begin{array}{l} (\hat{\mathbf{q}}, \mathbf{R}, m) \in \mathbf{C}_m \cap \mathbf{C}_1 \\ (\hat{\mathbf{q}}, \mathbf{R}, m) \in \mathbf{D}_1 \\ (\hat{\mathbf{q}}, \mathbf{R}, m) \in \mathbf{D}_m \end{array} \quad (18)$$

with continuous input $\mathbf{R} : \mathbb{R}_{\geq 0} \mapsto \text{SO}(3)$ and output

$$\vartheta := \left\{ \begin{array}{l} \varphi^{-1}(m\Phi(\hat{\mathbf{q}}, \mathbf{R})) \\ \emptyset \end{array} \right. , \quad \begin{array}{l} (\hat{\mathbf{q}}, \mathbf{R}, m) \in \mathbf{C}_m \cap \mathbf{C}_1 \\ (\hat{\mathbf{q}}, \mathbf{R}, m) \notin \mathbf{C}_m \cap \mathbf{C}_1 \end{array} \quad (19)$$

In the event of the conditions for \mathbf{D}_m and \mathbf{D}_1 being concurrently met, $(\hat{\mathbf{q}}, \mathbf{R}, m) \in \mathbf{D}_m \cap \mathbf{D}_1$, the formulation allows for either jump. Anticipating this two-fold possibility is required to ensure the fulfillment of the hybrid basic conditions. To study the properties of this hybrid algorithm, consider the autonomous system \mathcal{H}_ϑ^* characterized by

$$\mathcal{H}_\vartheta^* \left\{ \begin{array}{l} \dot{\hat{\mathbf{q}}} = 0, \quad \dot{\mathbf{R}} \in \mathbf{R} [K\mathbb{B}^3]_\times, \quad \dot{m} = 0 \\ \hat{\mathbf{q}}^+ \in \Phi(\hat{\mathbf{q}}, \mathbf{R}), \quad \mathbf{R}^+ = \mathbf{R}, \quad m^+ = m \\ \hat{\mathbf{q}}^+ = \hat{\mathbf{q}}, \quad \mathbf{R}^+ = \mathbf{R}, \quad m^+ = -m \end{array} \right. , \quad \begin{array}{l} (\hat{\mathbf{q}}, \mathbf{R}, m) \in \mathbf{C}_m \cap \mathbf{C}_1 \\ (\hat{\mathbf{q}}, \mathbf{R}, m) \in \mathbf{D}_1 \\ (\hat{\mathbf{q}}, \mathbf{R}, m) \in \mathbf{D}_m \end{array} \quad (20)$$

with the output ϑ specified in (19). In comparison with \mathcal{H}_ϑ , the latter system also encapsulates the dynamics of trajectories in $\text{SO}(3)$. [Lemma 1](#) details and demonstrates a few key attributes of the hybrid system \mathcal{H}_ϑ^* .

Lemma 1. *Let $\text{dist}(\hat{\mathbf{q}}, \mathcal{Q}(\mathbf{R}))|_{(0,0)} < 1$. The hybrid system \mathcal{H}_ϑ^* , described in (20), has the following properties:*

1. \mathcal{H}_ϑ^* is well-posed;
2. Every maximal solution to \mathcal{H}_ϑ^* is complete;
3. The output $\vartheta(t, j)$ verifies $\mathbf{R}_{\downarrow t}(t) = \mathcal{R}_\vartheta(\vartheta_{\downarrow t}(t))$
4. For any solution $(\hat{\mathbf{q}}, \mathbf{R}, m)(t, j)$, the output verifies $\|\vartheta(t, j)\| \leq 1 + \delta$.

Proof. The sets \mathbf{C}_1 , \mathbf{C}_m , \mathbf{D}_1 , and \mathbf{D}_m are closed. Since the intersection of closed sets is closed and the union of two closed sets is closed as well, the flow and jump maps, $\mathbf{C}_1 \cap \mathbf{C}_m$ and $\mathbf{D}_1 \cup \mathbf{D}_m$, respectively, are closed. The differential inclusion $\dot{\mathbf{R}} \in \mathbf{R} [K\mathbb{B}^3]_\times$ comprises a nonempty, outer-semicontinuous, locally bounded, and convex-valued map. From ([Mayhew et al., 2013](#), Theorem 7), the map $\Phi(\hat{\mathbf{q}}, \mathbf{R})$ is nonempty, outer semicontinuous, and locally bounded. Further, the difference equations are given by continuous functions. Thus, the hybrid system \mathcal{H}_ϑ^* verifies the hybrid basic conditions stated in ([Goebel et al., 2012](#), Assumption 6.5). Therefore, it follows from ([Goebel et al., 2012](#), Theorem 6.30) that \mathcal{H}_ϑ^* is well-posed.

Focusing on the completeness of the maximal solutions, by virtue of the set $(\mathbf{C}_1 \cap \mathbf{C}_m) \cup (\mathbf{D}_1 \cup \mathbf{D}_m) = \mathbb{S}^3 \times \text{SO}(3) \times \{-1, 1\}$ being compact, every solution is

bounded and, consequently, does not escape to infinity. Furthermore, any jump from $\mathbf{D}_1 \cup \mathbf{D}_m$ lands at a point in $(\mathbf{C}_1 \cap \mathbf{C}_m) \cup (\mathbf{D}_1 \cup \mathbf{D}_m)$. Therefore, every maximal solution is complete.

In virtue of $\mathcal{R}_\vartheta : \mathbb{R}^3 \mapsto \text{SO}(3)$ being a covering map, it follows from (Munkres, 2000, Lemma 54.1) that, for each fixed $j \in \mathbb{N}$, a given continuous path $\mathbf{R}_{\downarrow t} : \mathcal{T}_j \mapsto \text{SO}(3)$ satisfying $\mathbf{R}_{\downarrow t}(\min\{\mathcal{T}_j\}) = \mathcal{R}_\vartheta(\vartheta_{\downarrow t}(\min\{\mathcal{T}_j\}))$ has a unique lifting to a continuous path $\vartheta_{\downarrow t}(t)$ in the covering space \mathbb{R}^3 verifying $\vartheta_{\downarrow t}(\min\{\mathcal{T}_j\}) = \varphi^{-1}(m\Phi(\hat{\mathbf{q}}, \mathbf{R}))|_{(\min\{\mathcal{T}_j\}, j)}$. With this in mind, invariably, the ensuing step is to demonstrate that for $(t, j) \in \mathcal{T}_j \times j$, the lifted path indeed verifies $\vartheta_{\downarrow t}(t) = \varphi^{-1}(m\Phi(\hat{\mathbf{q}}, \mathbf{R}))|_{(t, j)}$. In this direction, suppose that, for $(\hat{\mathbf{q}}, \mathbf{R}, m) \in \mathbf{C}_m \cap \mathbf{C}_1$, a continuous $\mathbf{R}_{\downarrow t}(t) : \mathcal{T}_j \mapsto \text{SO}(3)$, and a continuous $\vartheta_{\downarrow t}(t) : \mathcal{T}_j \mapsto \mathbb{R}^3$ satisfying $\mathcal{R}_\vartheta(\vartheta_{\downarrow t}(t)) = \mathbf{R}_{\downarrow t}(t)$, there exists an instant $t' \in \mathcal{T}_j$ such that $\varphi^{-1}(m_{\downarrow t}(t')\Phi(\hat{\mathbf{q}}_{\downarrow t}(t'), \mathbf{R}_{\downarrow t}(t'))) = \Upsilon(\vartheta_{\downarrow t}(t'))$. Note that the latter equality is equivalent to $\varphi(\vartheta_{\downarrow t}(t')) = -\Phi(\hat{\mathbf{q}}_{\downarrow t}(t'), \mathbf{R}_{\downarrow t}(t'))$, which would imply that either $1 + \hat{\mathbf{q}}_{\downarrow t}^\top(t')\varphi(\vartheta_{\downarrow t}(t')) > 1$ or $m_{\downarrow t}(t') = -m_{\downarrow t}(\min\{\mathcal{T}_j\})$. Since the function $(1 + \hat{\mathbf{q}}^\top \mathbf{q}) : \mathbb{S}^3 \times \mathbb{S}^3 \mapsto \mathbb{R}$ is continuous, the inequality would translate to the existence of an instant $t^* \in [\min\{\mathcal{T}_j\}, t']$ such that $\text{dist}(\hat{\mathbf{q}}_{\downarrow t}(t^*), \mathcal{Q}(\mathbf{R}_{\downarrow t}(t^*))) = 1$. Alternatively, $m_{\downarrow t}(t') = -m_{\downarrow t}(\min\{\mathcal{T}_j\})$ presupposes the existence of an instant $t^* \in [\min\{\mathcal{T}_j\}, t']$ such that $\|\varphi^{-1}(m_{\downarrow t}(t^*)\Phi(\hat{\mathbf{q}}_{\downarrow t}(t^*), \mathbf{R}_{\downarrow t}(t^*)))\| > 1 + \delta$. Thus, given that the function $\Phi(\hat{\mathbf{q}}, R)$ is double-valued for $\text{dist}(\hat{\mathbf{q}}, \mathcal{Q}(\mathbf{R})) = 1$, both scenarios would violate the flow assumption $(\hat{\mathbf{q}}, \mathbf{R}, m) \in \mathbf{C}_m \cap \mathbf{C}_1$. Hence, for $(t, j) \in \mathcal{T}_j \times j$, the map composition $\varphi^{-1}(m\Phi(\hat{\mathbf{q}}, \mathbf{R}))$ is continuous and the lifted path satisfies $\vartheta(t, j) = \varphi^{-1}(m\Phi(\hat{\mathbf{q}}, \mathbf{R}))|_{(t, j)}$. As a result, for a fixed $j \in \mathbb{N}$, the output $\vartheta(t, j)$ verifies $\mathbf{R}_{\downarrow t}(t) = \mathcal{R}_\vartheta(\vartheta_{\downarrow t}(t))$. To examine the behaviour of the output during jumps, the following property of the map \mathcal{R}_ϑ is exploited:

$$\mathcal{R}_\vartheta(\vartheta') = \mathcal{R}_\vartheta(\vartheta) \quad \text{iff} \quad \vartheta' = \Upsilon(\vartheta)$$

Let $\{(t, j), (t, j+1)\} \subset \text{dom}(\hat{\mathbf{q}}, \mathbf{R}, m)$. There are two scenarios for $\vartheta(t, j+1)$: the jump either stems from the fulfilment of the condition defining \mathbf{D}_m , yielding $\vartheta(t, j+1) = \varphi^{-1}(-m\Phi(\hat{\mathbf{q}}, \mathbf{R}))|_{(t, j)}$, or from the verification of the inequality governing \mathbf{D}_1 , resulting in $\vartheta(t, j+1) = \varphi^{-1}(m\Phi(\Phi(\hat{\mathbf{q}}, \mathbf{R}), \mathbf{R}))|_{(t, j)}$. Regarding the first scenario, observe that the map φ satisfies the equality

$$\varphi^{-1}(-m\Phi(\hat{\mathbf{q}}, \mathbf{R}))|_{(t, j)} = \Upsilon(\varphi^{-1}(m\Phi(\hat{\mathbf{q}}, \mathbf{R}))|_{(t, j)}) \quad (21)$$

Thus, $\vartheta(t, j+1) = \Upsilon(\vartheta(t, j))$, and, recalling (2), $\mathcal{R}_\vartheta(\vartheta(t, j+1)) = \mathcal{R}_\vartheta(\vartheta(t, j))$. Concerning the second scenario, in virtue of the assumption $\text{dist}(\hat{\mathbf{q}}, \mathcal{Q}(\mathbf{R}))|_{(0,0)} < 1$ and, according to (Mayhew et al., 2013, Theorem 7), \mathbf{C}_1 being invariant, it follows from (Mayhew et al., 2013, Lemma 3) that a jump out of \mathbf{D}_1 yields $\vartheta(t, j) = \vartheta(t, j+1)$. Hence, one has $\mathcal{R}_\vartheta(\vartheta(t, j+1)) = \mathcal{R}_\vartheta(\vartheta(t, j))$ as well for this jump scenario. Therefore, the map $\mathcal{R}_\vartheta(\vartheta(t, j))$ is constant during jumps. This conclusion, in conjunction with the fact that, for every flow, exists a unique path-lifting $\vartheta_{\downarrow t}(t)$ of $\mathbf{R}_{\downarrow t}(t)$ satisfying $\mathcal{R}_\vartheta(\vartheta_{\downarrow t}(\min\{\mathcal{T}_j\})) = \mathbf{R}_{\downarrow t}(\min\{\mathcal{T}_j\})$ with $\vartheta_{\downarrow t}(\min\{\mathcal{T}_j\}) = \varphi^{-1}(m\Phi(\hat{\mathbf{q}}, \mathbf{R}))|_{(\min\{\mathcal{T}_j\}, j)}$, allows stating that the output $\vartheta(t, j)$ verifies $\mathbf{R}_{\downarrow t}(t) = \mathcal{R}_\vartheta(\vartheta_{\downarrow t}(t))$ for all $(t, j) \in \text{dom}(\hat{\mathbf{q}}, \mathbf{R}, m)$.

In view of the above, the output $\boldsymbol{\vartheta}$ is constant during jumps from \mathbf{D}_1 and its norm satisfies $\|\boldsymbol{\vartheta}\| \leq 1 + \delta$ after a jump from \mathbf{D}_m . Furthermore, notice that $\{(t, j) : \|\varphi^{-1}(m\Phi(\hat{\mathbf{q}}, \mathbf{R}))\| > 1 + \delta\} \subset \{(0, 0)\}$ and that this initial condition would mean $(\hat{\mathbf{q}}, \mathbf{R}, m)|_{(0,0)} \in \mathbf{D}_m$. Thus, given the definition of the output $\boldsymbol{\vartheta}$, provided in (19), the bound $\|\boldsymbol{\vartheta}(t, j)\| \leq 1 + \delta$ is attained. \square

3 Equivalence of stability results in the covering and base spaces

The previous section discussed the design and properties of a hybrid approach for lifting a path from the base space $\text{SO}(3)$ to the covering space $\bar{\mathbb{R}}^3$. Now, considering this methodology, the current section aims to assess the equivalence of stability between a closed-loop hybrid system that encompasses the differential equations of the rigid body, detailed in (1), and the hybrid path-lifting algorithm, and a hybrid closed-loop system that encapsulates the dynamics of the rigid body attitude expressed in terms of MRP, which comprise (1b) and (6). Within this framework, consider the MRP-based controller that has $\boldsymbol{\rho} \in \boldsymbol{\Lambda} \subset \mathbb{R}^n$ as state, $\boldsymbol{\vartheta}$ and $\boldsymbol{\omega}$ as inputs, and the torque $\boldsymbol{\tau}(\boldsymbol{\vartheta}, \boldsymbol{\omega}, \boldsymbol{\rho}) : \bar{\mathbb{R}}^3 \times \mathbb{R}^3 \times \boldsymbol{\Lambda} \mapsto \mathbb{R}^3$ as output. The dynamics of the state $\boldsymbol{\rho}$ are governed by the differential equation

$$\dot{\boldsymbol{\rho}} = \mathbf{f}(\boldsymbol{\vartheta}, \boldsymbol{\omega}, \boldsymbol{\rho}). \quad (22)$$

Due to the equivalence between the shortest rotational direction available and the MRP set with the lowest norm, MRP-based controllers do not require additional control mechanisms to determine the mentioned direction as it exploits this unique feature to prevent the unwinding phenomenon (see, for instance, Martins et al. (2021)). Hence, instead of the controller state having a discrete evolution, the attitude representation jumps by selectively transitioning between the original and shadow sets. Conversely, hybrid quaternion-based solutions rely on a discrete logic state, whose update depends on the scalar component of the quaternion, to impose the shortest rotation sought (Mayhew et al. (2011); Casau et al. (2015)).

The first closed-loop hybrid system, which consists of an interconnection between the rigid-body dynamic model (1), the output $\boldsymbol{\tau}(\boldsymbol{\vartheta}, \boldsymbol{\omega}, \boldsymbol{\rho}) : \bar{\mathbb{R}}^3 \times \mathbb{R}^3 \times \boldsymbol{\Lambda} \mapsto \mathbb{R}^3$ and dynamics (22) of the MRP-based controller, and the hybrid algorithm \mathcal{H}_ϑ , is denoted by $\mathcal{H}_1 := (\mathbf{C}_1, \mathbf{F}_1, \mathbf{D}_1, \mathbf{G}_1)$, has the vector $\mathbf{x}_1 := (\mathbf{R}_1, \hat{\mathbf{q}}_1, m_1, \boldsymbol{\omega}_1, \boldsymbol{\rho}_1) \in \chi_1 := \text{SO}(3) \times \mathbb{S}^3 \times \{-1, 1\} \times \mathbb{R}^3 \times \boldsymbol{\Lambda}$ as state, and is defined as

$$\mathbf{C}_1(\mathbf{x}_1) := \{\mathbf{x}_1 \in \chi_1 : (\mathbf{R}_1, \hat{\mathbf{q}}_1, m_1) \in \mathbf{C}_m \cap \mathbf{C}_1\} \quad (23a)$$

$$\mathbf{F}_1(\mathbf{x}_1) := \begin{cases} \dot{\mathbf{R}}_1 = \mathbf{R}_1[\boldsymbol{\omega}_1]_\times, & \dot{\hat{\mathbf{q}}}_1 = 0, & \dot{m}_1 = 0, \\ \mathbf{J}\dot{\boldsymbol{\omega}}_1 = [\mathbf{J}\boldsymbol{\omega}_1]_\times \boldsymbol{\omega}_1 + \boldsymbol{\tau}(\boldsymbol{\vartheta}^{-1}(m_1 \boldsymbol{\Phi}(\hat{\mathbf{q}}_1, \mathbf{R}_1)), \boldsymbol{\omega}_1, \boldsymbol{\rho}_1), & \\ \dot{\boldsymbol{\rho}}_1 = \mathbf{f}(\boldsymbol{\vartheta}_1, \boldsymbol{\omega}_1, \boldsymbol{\rho}_1) & \end{cases} \quad (23b)$$

$$\mathbf{D}_1(\mathbf{x}_1) := \{\mathbf{x}_1 \in \chi_1 : (\mathbf{R}_1, \hat{\mathbf{q}}_1, m_1) \in \mathbf{D}_m \cup \mathbf{D}_1\} \quad (23c)$$

$$\mathbf{G}_1(\mathbf{x}_1) := \begin{cases} \left(\begin{array}{l} \mathbf{R}_1^+ = \mathbf{R}_1, & \hat{\mathbf{q}}_1^+ \in \boldsymbol{\Phi}(\hat{\mathbf{q}}_1, \mathbf{R}_1), \\ m_1^+ = m_1, & \boldsymbol{\omega}_1^+ = \boldsymbol{\omega}_1, \\ \boldsymbol{\rho}_1^+ = \boldsymbol{\rho}_1 \end{array} \right), & (\mathbf{R}_1, \hat{\mathbf{q}}_1, m_1) \in \mathbf{D}_1 \\ \left(\begin{array}{l} \mathbf{R}_1^+ = \mathbf{R}_1, & \hat{\mathbf{q}}_1^+ = \hat{\mathbf{q}}_1, \\ m_1^+ = -m_1, & \boldsymbol{\omega}_1^+ = \boldsymbol{\omega}_1, \\ \boldsymbol{\rho}_1^+ = \boldsymbol{\rho}_1 \end{array} \right), & (\mathbf{R}_1, \hat{\mathbf{q}}_1, m_1) \in \mathbf{D}_m \end{cases} \quad (23d)$$

Notice that the hybrid system \mathcal{H}_1 behaves similarly to the lifting system \mathcal{H}_ϑ in terms of flows and jumps. As previously discussed, the primary purpose lies in evaluating the equivalence of stability between the solutions of the hybrid system \mathcal{H}_1 and another that resorts to the MRP description to model the attitude dynamics. Since MRP-based solutions found in the literature are devised directly on \mathbb{R}^3 without explicitly including a lifting system in the control architecture, the second closed-loop hybrid system, characterized by the data $\mathcal{H}_2 := (\mathbf{C}_2, \mathbf{F}_2, \mathbf{D}_2, \mathbf{G}_2)$, is strictly composed of (6), (1b), and (22). With this in mind, let $\mathbf{x}_2 := (\vartheta_2, \omega_2, \rho_2) \in \mathcal{X}_2 := \mathbb{R}^3 \times \mathbb{R}^3 \times \mathbf{A}$ define the state vector in order to formalize the hybrid system \mathcal{H}_2 as follows

$$\mathbf{C}_2(\mathbf{x}_2) := \{\mathbf{x}_2 \in \mathcal{X}_2 : \|\vartheta_2\| \leq 1 + \delta\} \quad (24a)$$

$$\mathbf{F}_2(\mathbf{x}_2) := \begin{cases} \dot{\vartheta}_2 = \mathbf{T}(\vartheta_2)\omega_2 \\ \mathbf{J}\dot{\omega}_2 = [\mathbf{J}\omega_2]_{\times}\omega_2 + \tau(\vartheta_2, \omega_2, \rho_2) \\ \dot{\rho}_2 = \mathbf{f}(\vartheta_2, \omega_2, \rho_2) \end{cases} \quad (24b)$$

$$\mathbf{D}_2(\mathbf{x}_2) := \{\mathbf{x}_2 \in \mathcal{X}_2 : \|\vartheta_2\| \geq 1 + \delta\} \quad (24c)$$

$$\mathbf{G}_2(\mathbf{x}_2) := \begin{cases} \vartheta_2^+ = \Upsilon(\vartheta_2) \\ \omega_2^+ = \omega_2 \\ \rho_2^+ = \rho_2 \end{cases} \quad (24d)$$

To lay the groundwork for comparing the stability of the hybrid systems \mathcal{H}_1 and \mathcal{H}_2 , Lemma 2 establishes parallelisms between the solutions of these two systems. Inspired by the approach proposed in (Mayhew et al., 2013, Lemma 8), the proof of this Lemma follows a recursive procedure to construct the solution of one of the hybrid systems and its hybrid time domain in terms of the solution of the other. Bear in mind that \mathcal{H}_1 encapsulates the jumps caused by the update of the memory state $\hat{\mathbf{q}}$ and by the MRP norm, whereas \mathcal{H}_2 only encompasses the latter. In each step, the approach verifies whether the constructed solution complies with the flow and jump dynamics of \mathcal{H}_2 .

Lemma 2. *Let $\text{dist}(\hat{\mathbf{q}}_1, \mathcal{Q}(\mathbf{R}_1))|_{(0,0)} < 1$. For every solution \mathbf{x}_1 to \mathcal{H}_1 , there exists a solution \mathbf{x}_2 to \mathcal{H}_2 that, for every $(t, j) \in \text{dom } \mathbf{x}_1$, yields*

$$(\mathbf{R}_1, \varphi^{-1}(m_1 \Phi(\hat{\mathbf{q}}_1, \mathbf{R}_1)), \omega_1, \rho_1)|_{(t,j)} = (\mathcal{R}_\vartheta(\vartheta_2), \vartheta_2, \omega_2, \rho_2)|_{(t,j')}, \quad (25)$$

with $(t, j') \in \text{dom } \mathbf{x}_2$ and $j' \in \mathbb{N}$ satisfying $j' < j$. Inversely, for every solution \mathbf{x}_2 to \mathcal{H}_2 , there exists a solution \mathbf{x}_1 to \mathcal{H}_1 such that, for every $(t, j') \in \text{dom } \mathbf{x}_2$, (25) holds with $(t, j) \in \text{dom } \mathbf{x}_1$ and $j > j'$.

Proof. Firstly, observe that, given the assumption $\text{dist}(\hat{\mathbf{q}}_1, \mathcal{Q}(\mathbf{R}_1))|_{(0,0)} < 1$ and (Mayhew et al., 2013, Theorem 7), the function $\Phi(\hat{\mathbf{q}}_1, \mathbf{R}_1)|_{(t,j)}$, and, consequently, $\varphi^{-1}(m_1 \Phi(\hat{\mathbf{q}}_1, \mathbf{R}_1))|_{(t,j)}$, are single-valued for all $(t, j) \in \text{dom } \mathbf{x}_1$. For the purpose of recursively expressing the solution \mathbf{x}_2 in terms of \mathbf{x}_1 , let $(t_0^\vartheta, j_0^\vartheta) = (0, 0)$. The, for each $i \in \mathbb{N}$, let $(t_{i+1}^\vartheta, j_{i+1}^\vartheta) \in \text{dom } \mathbf{x}_1$, given by

$$\begin{aligned} (t_{i+1}^\vartheta, j_{i+1}^\vartheta) &= \min\{(t, j) \in \text{dom } \mathbf{x}_1 : (t, j-1) \in \text{dom } \mathbf{x}_1, j > j_i^\vartheta, \\ &\quad \hat{\mathbf{q}}(t, j-1) = \hat{\mathbf{q}}(t, j), m(t, j-1) = -m(t, j)\}, \end{aligned} \quad (26)$$

denote the hybrid time instant immediately after the $(i + 1)^{\text{th}}$ jump triggered by the MRP norm. The minimum of this set is computed based on a natural way of ordering satisfying: for $(t, j), (t', j') \in \text{dom } \mathbf{x}_1$, $(t, j) \preceq (t', j')$ if $t \leq t'$ or $t = t'$ and $j \leq j'$. There are two possible outcomes for each $(t_{i+1}^\vartheta, j_{i+1}^\vartheta)$: either $(t_{i+1}^\vartheta, j_{i+1}^\vartheta) \neq \emptyset$, corresponding to the case in which an MRP jump indeed occurs, or $(t_{i+1}^\vartheta, j_{i+1}^\vartheta) = \emptyset$, indicating that there are no further jumps caused by the MRP vector norm. Starting with the former case, for each $i \in \mathbb{N}$, the hybrid time domain of \mathbf{x}_2 is recursively constructed through

$$\{(t, j) \in \text{dom } \mathbf{x}_2 : (t, j) \preceq (t_{i+1}^\vartheta, i + 1)\} = \left(\bigcup_{k=0}^i ([t_k^\vartheta, t_{k+1}^\vartheta], k) \right) \cup (t_{i+1}^\vartheta, i + 1) \quad (27)$$

and the solution \mathbf{x}_2 , for every $(t, j) \in \text{dom } \mathbf{x}_1$ verifying $t \in [t_i^\vartheta, t_{i+1}^\vartheta]$ and $j_i^\vartheta \leq j \leq j_{i+1}^\vartheta$, is defined as

$$\mathbf{x}_2(t, i) = (\varphi^{-1}(m_1 \Phi(\hat{\mathbf{q}}_1, \mathbf{R}_1)), \boldsymbol{\omega}_1, \boldsymbol{\rho}_1) \Big|_{(t, j)} \quad (28)$$

To verify the compliance of (28) with the jump dynamics of \mathcal{H}_2 , observe that, for the $(i + 1)^{\text{th}}$ jump due to the MRP norm, one has

$$\mathbf{x}_2(t_{i+1}^\vartheta, i) = (\varphi^{-1}(m_1 \Phi(\hat{\mathbf{q}}_1, \mathbf{R}_1)), \boldsymbol{\omega}_1, \boldsymbol{\rho}_1) \Big|_{(t_{i+1}^\vartheta, j_{i+1}^\vartheta - 1)} \quad (29)$$

$$\mathbf{x}_2(t_{i+1}^\vartheta, i + 1) = (\varphi^{-1}(m_1 \Phi(\hat{\mathbf{q}}_1, \mathbf{R}_1)), \boldsymbol{\omega}_1, \boldsymbol{\rho}_1) \Big|_{(t_{i+1}^\vartheta, j_{i+1}^\vartheta)} \quad (30)$$

The jump dynamics of \mathcal{H}_1 combined with the property (21) leads to

$$\mathbf{x}_2(t_{i+1}^\vartheta, i + 1) = (\Upsilon(\boldsymbol{\vartheta}_2), \boldsymbol{\omega}_2, \boldsymbol{\rho}_2) \Big|_{(t_{i+1}^\vartheta, i)} \quad (31)$$

Therefore, the solution (28) verifies the jump dynamics of \mathcal{H}_2 for each pair $\{(t, j), (t, j + 1)\} \in \text{dom } \mathbf{x}_2$ satisfying $(t, j) \preceq (t_{i+1}^\vartheta, i)$. Regarding the flow dynamics, first, it is worth highlighting that the covering map $\mathcal{R}_\vartheta : \bar{\mathbb{R}}^3 \mapsto \text{SO}^3$ is everywhere a local diffeomorphism and, thus, for every element $\boldsymbol{\vartheta} \in \bar{\mathbb{R}}^3$, the open neighborhood of $\boldsymbol{\vartheta}$ is diffeomorphic to an open neighborhood of an element $\mathcal{R}_\vartheta(\boldsymbol{\vartheta}) = \mathbf{R} \in \text{SO}(3)$, having, thereby, equivalent local differentiable structures. In addition, notice that, if $j_i^\vartheta < j_{i+1}^\vartheta - 1$, the hybrid system \mathcal{H}_1 jumps to update the memory state $\hat{\mathbf{q}}_1$ for $t \in [t_i^\vartheta, t_{i+1}^\vartheta]$. Nonetheless, as demonstrated in Lemma 1, the equality $\varphi^{-1}(m_1 \Phi(\hat{\mathbf{q}}_1, \mathbf{R}_1)) \Big|_{(t, j)} = \varphi^{-1}(m_1 \Phi(\hat{\mathbf{q}}_1, \mathbf{R}_1)) \Big|_{(t, j+1)}$ holds when updates of the memory state $\hat{\mathbf{q}}_1$ occur and, consequently, the solution proposed in (28) remains constant during these jumps. Furthermore, from the proof of Lemma 1 it also follows that, for all $(t, j) \in \text{dom } \mathbf{x}_1$ satisfying $t \in [t_i^\vartheta, t_{i+1}^\vartheta]$ and $j_i^\vartheta \leq j \leq j_{i+1}^\vartheta$, the map $\varphi^{-1}(m_1 \Phi(\hat{\mathbf{q}}_1, \mathbf{R}_1)) \Big|_{(t, j)}$ is continuous and verifies $\mathcal{R}_\vartheta(\varphi^{-1}(m_1 \Phi(\hat{\mathbf{q}}_1, \mathbf{R}_1)) \Big|_{(t, j)}) = \mathbf{R}_1(t, j)$. Thus, $\boldsymbol{\vartheta}_2(t, i) = \varphi^{-1}(m_1 \Phi(\hat{\mathbf{q}}_1, \mathbf{R}_1)) \Big|_{(t, j)}$, for all $(t, j) \in \text{dom } \mathbf{x}_1$ satisfying $t \in [t_i^\vartheta, t_{i+1}^\vartheta]$ and $j_i^\vartheta \leq j \leq j_{i+1}^\vartheta$, yields $\mathbf{R}_1(t, j) = \mathcal{R}_\vartheta(\boldsymbol{\vartheta}_2(t, i))$ and complies with the kinematic expression (6). Hence, on the basis of these results and in light of the states $\boldsymbol{\omega}_2$

and $\boldsymbol{\rho}_2$ being equal to the counterpart states of \mathcal{H}_1 , being governed by identical differential equations, and being constant during jumps, one concludes that the solution (28) verifies the flow dynamics of \mathcal{H}_2 for each $(t, j) \in \text{dom } \mathbf{x}_2$ satisfying $(t, j) \preceq (t_{i+1}^\vartheta, i+1)$. In the event of $(t_{i+1}^\vartheta, j_{i+1}^\vartheta) \neq \emptyset \forall i \in \mathbb{N}$, the domain of the solution $\mathbf{x}_2(t, j)$ is given by

$$\text{dom } \mathbf{x}_2 = \bigcup_{k=0}^{\infty} ([t_k^\vartheta, t_{k+1}^\vartheta], k), \quad (32)$$

and, in virtue of the foregoing considerations, the expression (28) describes a solution to \mathcal{H}_2 for all $(t, j) \in \text{dom } \mathbf{x}_2$. Moreover, for every $(t, j) \in \text{dom } \mathbf{x}_1$, there exists $(t, j') \in \text{dom } \mathbf{x}_2$, with $j' \leq j$, such that (25) holds.

As previously discussed, the second case anticipates the scenario in which there exists an $i' \in \mathbb{N}$ such that $(t_{i'+1}^\vartheta, j_{i'+1}^\vartheta) = \emptyset$. In this context, the domain of \mathbf{x}_2 is defined as

$$\text{dom } \mathbf{x}_2 = \begin{cases} ([0, \bar{T}(\mathbf{x}_1)], 0) & , \text{ for } i' = 0 \\ \left(\bigcup_{k=0}^{i'-1} ([t_k^\vartheta, t_{k+1}^\vartheta], k) \right) \cup ([t_{i'}^\vartheta, \bar{T}(\mathbf{x}_1)], i') & , \text{ otherwise} \end{cases} \quad (33)$$

The previous paragraph demonstrates that (28) yields a solution to \mathcal{H}_2 for every $\{(t, j)\} \in \text{dom } \mathbf{x}_2$ satisfying $(t, j) \preceq (t_{i'}^\vartheta, i')$. For every $(t, i') \in \text{dom } \mathbf{x}_2$ and every $(t, j) \in \text{dom } \mathbf{x}_2$ satisfying $j \geq j_{i'}^\vartheta$, one has

$$\mathbf{x}_2(t, i') = (\varphi^{-1}(m_1 \Phi(\hat{\mathbf{q}}_1, \mathbf{R}_1)), \boldsymbol{\omega}_1, \boldsymbol{\rho}_1) \Big|_{(t, j)} \quad (34)$$

By applying a reasoning similar to that followed to demonstrate that (28) verifies the hybrid dynamics of \mathcal{H}_2 for every $\{(t, j)\} \in \text{dom } \mathbf{x}_2$ satisfying $(t, j) \preceq (t_{i'}^\vartheta, i')$, one concludes that $\mathbf{x}_2 : \text{dom } \mathbf{x}_2 \mapsto \boldsymbol{\chi}_2$, defined by (28) in combination with (34), with $\text{dom } \mathbf{x}_2$ specified in (33), verifies the flow and jump dynamics of \mathcal{H}_2 , constituting, thereby, a solution to this hybrid system. Further, for every $(t, j) \in \text{dom } \mathbf{x}_1$, there exists $(t, j') \in \text{dom } \mathbf{x}_2$, with $j' \leq j$, such that (25) holds.

Having demonstrated the first part of the lemma, the proof of the second part is straightforward if one uses the previous sequence of arguments as a blueprint. To elaborate, this proof follows similarly by recursively constructing the solution to \mathcal{H}_1 in terms of the solution to \mathcal{H}_2 , with the minor nuance of adding the jumps that update the quaternion memory state $\hat{\mathbf{q}}_1$. \square

The relation provided in Lemma 2 allows one to develop a theoretical basis for bridging the stability results of the hybrid systems \mathcal{H}_1 and \mathcal{H}_2 . In this direction, by building on the previous results, Theorem 1 focuses on demonstrating that a feedback controller designed in the covering space $\bar{\mathbb{R}}^3$ yields identical stability results for a system defined in the MRP space and another defined in the base space $\text{SO}(3)$ when the latter resorts to the hybrid dynamic path-lifting algorithm \mathcal{H}_ϑ to lift the attitude representation from $\text{SO}(3)$ to $\bar{\mathbb{R}}^3$.

Theorem 1. *Let $\alpha \in]0, 1[$ and $\delta \in \mathbb{R}_{>0}$. Suppose that a compact set $\mathcal{A}_\vartheta \in \mathcal{X}_2$ is asymptotically stable for the hybrid system \mathcal{H}_2 with \mathcal{B}_ϑ as basin of attraction. Then, the compact*

$$\begin{aligned} \mathcal{A} = \{ & \mathbf{x}_1 \in \mathcal{X}_1 : (\varphi^{-1}(m_1 \Phi(\hat{\mathbf{q}}_1, \mathbf{R}_1)), \boldsymbol{\omega}_1, \boldsymbol{\rho}_1) \in \mathcal{A}_\vartheta, \\ & \|\varphi^{-1}(m_1 \Phi(\hat{\mathbf{q}}_1, \mathbf{R}_1))\| \leq 1 + \delta, \text{dist}(\hat{\mathbf{q}}_1, \mathcal{Q}(\mathbf{R}_1)) \leq \alpha \} \end{aligned}$$

is asymptotically stable for the hybrid system \mathcal{H}_1 with

$$\mathcal{B} = \{ \mathbf{x}_1 \in \mathcal{X}_1 : (\varphi^{-1}(m_1 \Phi(\hat{\mathbf{q}}_1, \mathbf{R}_1)), \boldsymbol{\omega}_1, \boldsymbol{\rho}_1) \in \mathcal{B}_\vartheta, \text{dist}(\hat{\mathbf{q}}_1, \mathcal{Q}(\mathbf{R}_1)) < 1 \}$$

as basin of attraction. Conversely, if the compact set \mathcal{A} is asymptotically stable for \mathcal{H}_1 with \mathcal{B} as basin of attraction, then the compact set \mathcal{A}_ϑ is asymptotically stable for the hybrid system \mathcal{H}_2 with \mathcal{B}_ϑ as basin of attraction.

Proof. The proof flows from combining the definitions of stable and attractive sets with the result presented in [Lemma 2](#). In this direction, to prove the first part of the theorem, assume that the compact set \mathcal{A}_ϑ is asymptotically stable for \mathcal{H}_2 . Then, according to ([Goebel et al., 2012](#), Definition 7.1), it follows that for every $\epsilon \in \mathbb{R}_{>0}$ there exists $\iota \in \mathbb{R}_{>0}$ satisfying $\iota \leq \epsilon$ such that each solution $\mathbf{x}_2(t, j)$ to \mathcal{H}_2 with $\|\mathbf{x}_2(0, 0)\|_{\mathcal{A}_\vartheta} < \iota$ yields $\|\mathbf{x}_2(t, j)\|_{\mathcal{A}_\vartheta} < \epsilon \forall (t, j) \in \text{dom } \mathbf{x}_2$. Furthermore, it also follows that $\mathbf{x}_2(0, 0) \in \mathcal{B}_\vartheta$ yields $\lim_{(t+j) \rightarrow \infty} \|\mathbf{x}_2(t, j)\|_{\mathcal{A}_\vartheta} = 0$. In light of [Lemma 2](#), for every solution \mathbf{x}_2 to \mathcal{H}_2 , there exists a solution \mathbf{x}_1 to \mathcal{H}_1 such that, for every $(t, j') \in \text{dom } \mathbf{x}_2$, (25) holds with $(t, j) \in \text{dom } \mathbf{x}_1$ and $j > j'$. Note that, one can assume, without sacrificing generality, that $\mathbf{x}_1(t, j)$ satisfies $\text{dist}(\hat{\mathbf{q}}_1, \mathcal{Q}(\mathbf{R}_1))|_{(0,0)} < 1$. Therefore, $\|\mathbf{x}_2(0, 0)\|_{\mathcal{A}_\vartheta} < \iota$ and $\mathbf{x}_2(0, 0) \in \mathcal{B}_\vartheta$ imply, respectively,

$$\| (\varphi^{-1}(m_1 \Phi(\hat{\mathbf{q}}_1, \mathbf{R}_1)), \boldsymbol{\omega}_1, \boldsymbol{\rho}_1) |_{(0,0)} \|_{\mathcal{A}_\vartheta} < \iota \quad (35a)$$

$$(\varphi^{-1}(m_1 \Phi(\hat{\mathbf{q}}_1, \mathbf{R}_1)), \boldsymbol{\omega}_1, \boldsymbol{\rho}_1) |_{(0,0)} \in \mathcal{B}_\vartheta \quad (35b)$$

Moreover, given the latter results, since \mathcal{A}_ϑ is stable and attractive from \mathcal{B}_ϑ for \mathcal{H}_ϑ , the equivalence described by (25) also presupposes that, for every $\epsilon \in \mathbb{R}_{>0}$, there exists $\iota \in \mathbb{R}_{>0}$ verifying $\iota \leq \epsilon$ such that any solution \mathbf{x}_1 to \mathcal{H}_1 satisfying (35a) yields $\| (\varphi^{-1}(m_1 \Phi(\hat{\mathbf{q}}_1, \mathbf{R}_1)), \boldsymbol{\omega}_1, \boldsymbol{\rho}_1) |_{(t,j)} \|_{\mathcal{A}_\vartheta} < \epsilon \forall (t, j) \in \text{dom } \mathbf{x}_1$, and every solution \mathbf{x}_1 to \mathcal{H}_1 satisfying (35b) leads to

$$\lim_{(t+j) \rightarrow \infty} \| (\varphi^{-1}(m_1 \Phi(\hat{\mathbf{q}}_1, \mathbf{R}_1)), \boldsymbol{\omega}_1, \boldsymbol{\rho}_1) |_{(t,j)} \|_{\mathcal{A}_\vartheta} = 0 \quad (36)$$

The properties of the map $\mathcal{R}_\vartheta : \bar{\mathbb{R}}^3 \mapsto \text{SO}(3)$ demonstrated in [section 1](#), namely, being a covering map and everywhere a local diffeomorphism, are instrumental inasmuch as these properties enable expressing a given open neighborhood of \mathcal{A} in terms of an open neighborhood of \mathcal{A}_ϑ . In this direction, let $\mathcal{U}^\epsilon \supset \mathcal{A}$ and $\mathcal{U}^\iota \supset \mathcal{A}$ denote open neighborhoods of \mathcal{A} defined as

$$\begin{aligned} \mathcal{U}^\epsilon = \{ & \mathbf{x}_1 \in \mathcal{X}_1 : \| (\varphi^{-1}(m_1 \Phi(\hat{\mathbf{q}}_1, \mathbf{R}_1)), \boldsymbol{\omega}_1, \boldsymbol{\rho}_1) |_{(t,j)} \|_{\mathcal{A}_\vartheta} < \epsilon, \\ & \|\varphi^{-1}(m_1 \Phi(\hat{\mathbf{q}}_1, \mathbf{R}_1))\| \leq 1 + \delta + \epsilon, \text{dist}(\hat{\mathbf{q}}_1, \mathcal{Q}(\mathbf{R}_1)) \leq \alpha + \epsilon \}, \end{aligned} \quad (37)$$

$$\begin{aligned} \mathcal{U}^\iota &= \{\mathbf{x}_1 \in \mathcal{X}_1 : \|(\varphi^{-1}(m_1 \Phi(\hat{\mathbf{q}}_1, \mathbf{R}_1)), \boldsymbol{\omega}_1, \boldsymbol{\rho}_1)|_{(t,j)}\|_{\mathcal{A}_\vartheta} < \iota, \\ &\quad \|\varphi^{-1}(m_1 \Phi(\hat{\mathbf{q}}_1, \mathbf{R}_1))\| \leq 1 + \delta + \iota, \text{dist}(\hat{\mathbf{q}}_1, \mathcal{Q}(\mathbf{R}_1)) \leq \alpha + \iota\} \end{aligned} \quad (38)$$

Note that, in virtue of the map Φ being double-valued for $\text{dist}(\hat{\mathbf{q}}_1, \mathcal{Q}(\mathbf{R}_1)) = 1$, the open neighborhoods \mathcal{U}^ϵ and \mathcal{U}^ι are defined for $\iota \leq \epsilon < 1 - \alpha$. Bearing in mind (Mayhew et al., 2013, Theorem 7) and Lemma 1, the initial condition $\mathbf{x}_1(0, 0) \in \mathcal{U}^\iota$ results in $\|\varphi^{-1}(m_1 \Phi(\hat{\mathbf{q}}_1, \mathbf{R}_1))|_{(t,j)}\| \leq 1 + \delta + \epsilon$ and $\text{dist}(\hat{\mathbf{q}}_1, \mathcal{Q}(\mathbf{R}_1))|_{(t,j)} \leq \alpha + \epsilon$ for all $(t, j) \in \text{dom } \mathbf{x}_1$. Hence, given the foregoing results, for every $\epsilon < 1 - \alpha$, there exists there exists $\iota \leq \epsilon$ such that any solution \mathbf{x}_1 to \mathcal{H}_1 satisfying $\mathbf{x}_1(0, 0) \in \mathcal{U}^\iota$ yields $\mathbf{x}_1(t, j) \in \mathcal{U}^\epsilon \forall (t, j) \in \text{dom } \mathbf{x}_1$. Thus, the compact set \mathcal{A} is stable for \mathcal{H}_1 . Furthermore, under the same reasoning and with particular emphasis on (36), it follows that $\mathbf{x}_1(0, 0) \in \mathcal{B}$ leads to $\lim_{(t+j) \rightarrow \infty} \|\mathbf{x}_1(t, j)\|_{\mathcal{A}} = 0$. Therefore, the compact set \mathcal{A} is asymptotically stable for \mathcal{H}_1 with \mathcal{B} as basin of attraction whenever the compact set \mathcal{A}_ϑ is asymptotically stable for \mathcal{H}_2 with \mathcal{B}_ϑ as basin of attraction.

To demonstrate the converse, suppose now that the set \mathcal{A} is asymptotically stable for \mathcal{H}_1 with \mathcal{B} as basin of attraction. Then, since for $\mathbf{x}_1(0, 0) \in \mathcal{B} \cup \mathcal{U}^\iota$ one has $\text{dist}(\hat{\mathbf{q}}_1, \mathcal{Q}(\mathbf{R}_1))|_{(0,0)} < 1$, in virtue of Lemma 2, for every solution \mathbf{x}_1 to \mathcal{H}_1 , there exists a solution \mathbf{x}_2 to \mathcal{H}_2 that, for every $(t, j) \in \text{dom } \mathbf{x}_1$, (25) holds with $(t, j') \in \text{dom } \mathbf{x}_2$ and $j' \in \mathbb{N}$ satisfying $j' < j$. In this way, $\mathbf{x}_1(0, 0) \in \mathcal{B}$ implies $\mathbf{x}_2(0, 0) \in \mathcal{B}_\vartheta$ and, since \mathcal{A} is attractive from \mathcal{B} , the equality (25) allows concluding that $\lim_{(t+j') \rightarrow \infty} \|\mathbf{x}_2(t, j')\|_{\mathcal{A}_\vartheta} = 0$. Similarly, stemming from (25), given that \mathcal{A} is stable, for any given ϵ satisfying $\epsilon < 1 - \alpha$, there exists ι , verifying $\iota \leq \epsilon$, such that $\mathbf{x}_1(0, 0) \in \mathcal{U}^\iota$ infers $\|\mathbf{x}_2(0, 0)\|_{\mathcal{A}_\vartheta} < \iota$ and $\|\mathbf{x}_2(t, j')\|_{\mathcal{A}_\vartheta} < \epsilon \forall (t, j') \in \text{dom } \mathbf{x}_2$. Consequently, under the assumption that the compact set \mathcal{A} is asymptotically stable for \mathcal{H}_1 with \mathcal{B} as basin of attraction, the compact set \mathcal{A}_ϑ is asymptotically stable for the hybrid system \mathcal{H}_2 with \mathcal{B}_ϑ as basin of attraction. \square

References

- P. Casau, R. G. Sanfelice, R. Cunha, D. Cabecinhas, and C. Silvestre. Robust global trajectory tracking for a class of underactuated vehicles. *Automatica*, 58:90–98, 2015.
- R. Goebel, R. G. Sanfelice, and A. Teel. *Hybrid dynamical systems: modeling, stability, and robustness*. Princeton University Press, 2012.
- J. L. Junkins and H. Schaub. *Analytical Mechanics of Space Systems*. American Institute of Aeronautics and Astronautics, 2009.
- J. M. Lee. *Introduction to Smooth Manifolds*. Springer, 2013.
- L. Martins, C. Cardeira, and P. Oliveira. Global trajectory tracking for quadrotors: An mrp-based hybrid backstepping strategy. In *2021 60th IEEE Conference on Decision and Control (CDC)*, pages 5759–5764, 2021.
- C. G. Mayhew, R. G. Sanfelice, and A. R. Teel. Quaternion-based hybrid control for robust global attitude tracking. *IEEE Transactions on Automatic control*, 56(11):2555–2566, 2011.
- C. G. Mayhew, R. G. Sanfelice, and A. R. Teel. On path-lifting mechanisms and unwinding in quaternion-based attitude control. *IEEE Transactions on Automatic Control*, 58(5):1179–1191, May 2013.
- J. R. Munkres. *Topology*, volume 2. Prentice Hall Upper Saddle River, 2000.